Sensors & Actuators: B. Chemical 444 (2025) 138418

Contents lists available at ScienceDirect

Sensors and Actuators: B. Chemical

journal homepage: www.elsevier.com/locate/snb

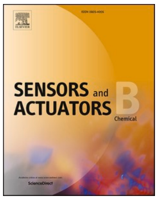

In vivo imaging and chemotherapy monitoring of breast cancer with β-galactosidase-activated fluorescence probe

Jingkang Li [a], Chen Zhao [a], Mo Ma [a,c], Lanyun Zhang [a], Wanqi Li [a], Pinyi Ma [a,*], Qiong Wu [b,*], Daqian Song [a,*]

[a] *College of Chemistry, Jilin Province Research Center for Engineering and Technology of Spectral Analytical Instruments, Jilin University, Qianjin Street 2699, Changchun 130012, China*
[b] *Key Laboratory of Pathobiology, Ministry of Education, Nanomedicine and Translational Research Center, The Third Bethune Hospital of Jilin University, Sendai Street 126, Changchun 130033, China*
[c] *School of Pharmacy, Jilin University, Qianjin Street 2699, Changchun 130012, China*

ARTICLE INFO

Keywords:
Fluorescent probe
β-gal
Breast cancer
Cell senescence
Palbociclib

ABSTRACT

Breast cancer is a major global health concern that necessitates early diagnosis and effective monitoring of therapeutic efficacy. β-galactosidase (β-gal) is a valuable biomarker linked to cellular senescence and tumor progression; however, existing detection probes frequently face challenges such as low water solubility, suboptimal fluorescence quantum yield, and insufficient stability in complex biological environments. To address these limitations, a novel fluorescence probe, QST-GAL, was developed by introducing a sulfonic acid group into a quinoline-based near-infrared dye to improve hydrophilicity and by incorporating a thiophene moiety to extend the conjugation system. The presence of these groups enhances the intramolecular charge transfer of the probe. Under optimal conditions, QST-GAL had a linear detection range of 2–28 U/mL and a low detection limit of 0.377 U/mL. Cellular assays confirmed the probe's ability to visualize breast cancer cells and monitor chemotherapy-induced senescence. Using a breast cancer mouse model, QST-GAL was successfully employed in *in vivo* tumor imaging, fluorescence-guided surgical resection, and accurate assessment of the Palbociclib's therapeutic effects. This probe offers a promising tool for both diagnosis and treatment monitoring of breast cancer.

1. Introduction

Breast cancer is among the most prevalent malignancies worldwide [1–4]. Despite major advances in all aspects of breast cancer treatment, early and accurate diagnosis, along with disease monitoring, remains central to improving patient survival and prognosis [5–7]. The discovery of various tumor-associated biomarkers has provided new opportunities for precise diagnosis and personalized treatment [8–10]. β-galactosidase (β-gal), an enzyme associated with cellular senescence and tumor progression, has become an important target for disease diagnosis and therapeutic monitoring [11–15]. Its activity is elevated in breast cancer and other tumor types and is closely linked to the senescence-associated secretory phenotype (SASP), a cellular state often induced by treatments such as chemotherapy and radiotherapy [16–18]. Therefore, β-gal activity serves as a valuable molecular marker for early breast cancer diagnosis and real-time tracking of tumor responses to therapy.

Small molecule-based fluorescence probes are essential tools for detecting β-gal activity [19–26]. These probes undergo β-gal-catalyzed hydrolysis reactions, generating strong fluorescent signals that enable tumor visualization and high-resolution imaging that provide molecular-level insights into disease progression and therapeutic efficacy [26–29]. Yuan et al. designed a β-galactosidase-activated fluorescence probe, NIR-βgal-2, with excellent sensitivity and affinity for β-gal and employed it to facilitate intraoperative guidance for breast tumor resection [30]. Additionally, Tan et al. reported a dual-parameter fluorescence probe for high-contrast cellular senescence imaging independent of cell origin or stress type [31]. These probes provide effective means for early cancer diagnosis and real-time monitoring of chemotherapy efficacy to help clinicians optimize their treatment plans and improve patient outcomes. Despite these advancements, it remains challenging to enhance the sensitivity, specificity, and biocompatibility of fluorescence probes for β-gal detection. The water solubility,

---

* Corresponding authors.
E-mail addresses: mapinyi@jlu.edu.cn (P. Ma), qiong_wu@jlu.edu.cn (Q. Wu), songdq@jlu.edu.cn (D. Song).

https://doi.org/10.1016/j.snb.2025.138418
Received 12 June 2025; Received in revised form 24 July 2025; Accepted 28 July 2025
Available online 28 July 2025

fluorescence quantum yield, and stability in complex biological environments of the existing probes often require optimization.

In this study, we designed and synthesized a novel near-infrared fluorescent dye, QST-OH, based on quinoline derivatives. By incorporating a thiophene group, we were able to enhance the electron delocalization and lower the excitation state energy, which caused a red shift in the fluorescence emission. By further modifying with a sulfonic acid group to introduce a quaternary ammonium structure, the water solubility and biocompatibility of the probe were improved [32]. β-galactose residues were then incorporated to generate the β-galactosidase-specific probe, QST-GAL, which can be employed in the rapid, accurate detection of β-gal activity *in vitro* and cellular imaging. The QST-GAL probe was successfully employed in *in situ* imaging of a breast cancer mouse model and monitoring tumor treatment. This work provides essential evidence for the application of the QST-GAL probe in breast cancer diagnosis and treatment monitoring.

2. Experimental methods

2.1. Materials and equipment

Detailed information regarding the reagents and instruments used in this study is provided in the Supplementary Material. The synthesis route for the compounds is shown in Fig. 1. Detailed procedures for the synthesis of Compound 1, Compound 2 and Compound 3 are also available in the Supplementary Material (Figure S1 – Figure S6).

Synthesis of QST-OH. Compound 2 (1.59 g, 6 mmol) and Compound 1 (1.02 g, 5 mmol) were added to a pressure-resistant reaction tube, followed by 20 mL of anhydrous ethanol (as a solvent). The mixture was stirred at 85℃ until the solution became transparent. After that, 20 μL of piperidine was added slowly to the mixture. The reaction was terminated when a solid was formed. The mixture was then cooled to room temperature. The solid was collected by filtration and dissolved in methanol:dichloromethane (v/v = 1:1). The resulting solution was purified by silica gel column chromatography using methanol:dichloromethane (v/v = 8:1) as the mobile phase, which yielded the brown solid QST-OH (651 mg, 28.2 % yield). ^{1}H NMR (600 MHz, DMSO-d_6) δ 9.99 (s, 1 H), 8.92 (d, $J = 9.1$ Hz, 1 H), 8.65 (d, $J = 9.0$ Hz, 1 H), 8.58 (d, $J = 9.1$ Hz, 1 H), 8.49 (d, $J = 15.2$ Hz, 1 H), 8.29 (d, $J = 8.3$ Hz, 1 H), 8.16 (d, $J = 4.0$ Hz, 1 H), 8.14 – 8.11 (m, 1 H), 7.88 (dd, $J = 15.3$, 7.7 Hz, 2 H), 7.63 (d, $J = 8.6$ Hz, 2 H), 7.58 (d, $J = 4.0$ Hz, 1 H), 6.89 – 6.87 (m, 2 H), 5.24 (s, 2 H), 2.81 (d, $J = 6.2$ Hz, 2 H), 1.63 (p, $J = 6.1$ Hz, 2 H). ^{13}C NMR (151 MHz, DMSO-d$_6$) δ 167.5, 159.1, 155.6, 151.8, 143.5, 141.0, 138.9, 138.0, 135.3, 130.6, 129.1, 128.2, 127.9, 124.9, 124.5, 120.9, 119.4, 116.6, 116.0, 67.9, 30.3, 11.3. MS data (LC-ESI-MS, m/z) for $C_{13}H_{16}NO_3S^+$ $[M+H]^+$: calculated, 452.0985; found:452.0984. (Figure S7-Figure S9)

Synthesis of QST-GAL. Compound 3 (0.156 g, 0.2 mmol) was dissolved in 10 mL of anhydrous methanol, and while stirring, a methanol solution of sodium methoxide (100 μL, 0.54 mmol) was added dropwise. The reaction was continued at room temperature, and the progress was monitored by TLC. After the reaction was complete, the solvent was removed under reduced pressure. The product was purified by silica gel column chromatography using dichloromethane:methanol:formic acid (v/v/v = 8:2:0.01) as the eluent. QST-GAL was obtained as a purplish-black solid (89 mg, 72.6 % yield). ^{1}H NMR (600 MHz, DMSO-d_6) δ 8.95 (d, $J = 9.1$ Hz, 1 H), 8.66 (d, $J = 9.1$ Hz, 1 H), 8.60 (d, $J = 9.2$ Hz, 1 H), 8.51 (d, $J = 15.2$ Hz, 1 H), 8.46 (s, 1 H), 8.17 (d, $J = 4.0$ Hz, 1 H), 8.14 (s, 1 H), 8.12 (s, 1 H), 7.92 – 7.87 (m, 2 H), 7.75 – 7.72 (m, 2 H), 7.67 (d, $J = 4.0$ Hz, 1 H), 7.14 (d, $J = 8.8$ Hz, 2 H), 5.26 (s, 2 H), 4.92 (d, $J = 7.7$ Hz, 1 H), 3.74 (d, $J = 3.4$ Hz, 1 H), 3.65 – 3.60 (m, 3 H), 3.60 – 3.55 (m, 3 H), 3.53 – 3.50 (m, 2 H), 3.44 (dd, $J = 9.5$, 3.4 Hz, 2 H), 2.86 – 2.83 (m, 2 H). ^{13}C NMR (151 MHz, DMSO-d_6) δ 158.6, 155.5, 143.8, 140.8, 138.7, 135.3, 135.1, 130.7, 127.6, 127.0, 125.6, 121.0, 119.5,

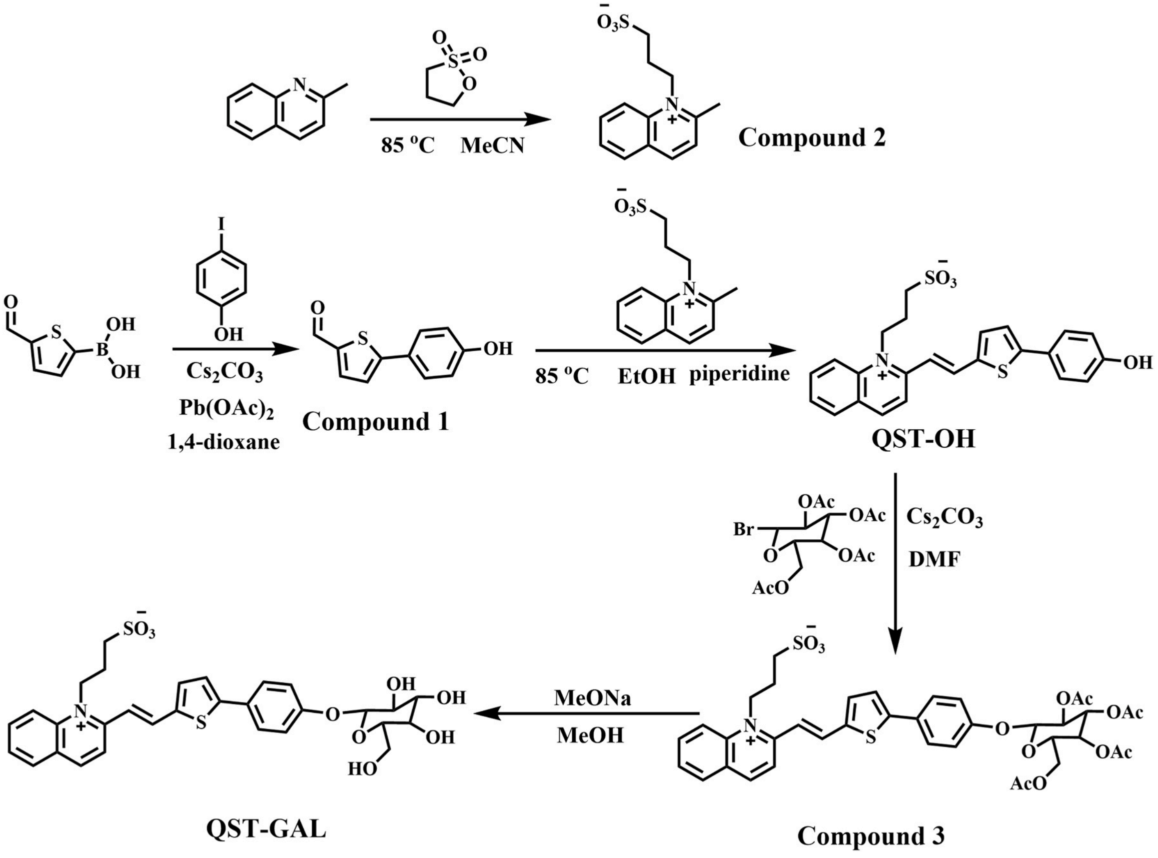

Fig. 1. Synthetic route of QST-OH and probe QST-GAL.

117.5, 116.5, 101.2, 76.1, 73.8, 70.7, 68.5, 60.8, 47.9. MS data (LC-ESI-MS, m/z) for $C_{13}H_{16}NO_3S^+$ $[M+H]^+$: calculated, 614.1513; found:614.1524. (Figure S10-Figure S12)

2.2. Detection of β-gal in solution

A 1 mM stock solution of QST-GAL was prepared in DMSO. To find the optimal conditions, various reaction parameters were systematically optimized as follows:

Reaction time optimization. Reactions containing 10 U/mL β-gal and 10 μM QST-GAL dissolved in phosphate-buffered saline (PBS, 10 mM, pH 7.4) were incubated at 37℃ for varying durations (0.3, 0.6, 0.9, 1.2, 1.5, 2.5, 3, 4, 5, and 10 min). The optimal reaction time was determined based on changes in the fluorescence signal.

pH condition optimization. PBS solutions at different pH values (4, 5, 6, 7, 7.4, 8, 9, 10, and 11) were prepared. Reactions containing 10 U/mL β-gal and 10 μM QST-GAL were incubated at 37℃ for 5 min. The pH that yielded the highest fluorescence signal was considered optimal.

Reaction temperature optimization. Mixtures containing 10 U/mL β-gal and 10 μM QST-GAL in PBS were incubated at various temperatures (25℃, 30℃, 37℃, 40℃, and 45℃) for 5 min. The temperature that resulted in the highest reaction efficiency was considered optimal.

Probe selectivity evaluation. Reactions containing 10 μM QST-GAL dissolved in PBS were incubated at 37℃ for 5 min. The selectivity of the probe toward β-gal was assessed by fluorescence spectroscopy.

Enzyme kinetics parameters determination. Solutions containing 10 U/mL β-gal and QST-GAL probe at various concentrations (1, 3, 5, 10, 15, 20, 40, 60, and 80 μM) were prepared in 10 mM PBS buffer, pH 7.4. The fluorescence intensity of each solution was recorded every 0.3 min at an excitation wavelength of 585 nm and an emission wavelength of 710 nm for 2 min. The initial reaction rates were determined based on the linear response range of the fluorescence intensity change curves. The reaction kinetic parameters were determined using the Michaelis-Menten and Lineweaver-Burk equations. The formula for calculating the enzyme catalytic constant is detailed in the supporting information.

2.3. Cell culture and imaging studies

4T1 mouse mammary tumor cells (iCell Bioscience) were cultured in DMEM supplemented with 10 % fetal bovine serum (FBS) and penicillin-streptomycin. The cells were maintained at 37℃ in an atmosphere humidified with 5 % CO_2. Imaging was performed using a Nikon AX laser scanning confocal microscope at an excitation wavelength of 500 nm and an emission wavelength of 700 nm.

Time-lapse imaging using QST-GAL. For time-lapse imaging, 4T1 cells were incubated with 10 μM QST-GAL, and the fluorescence changes were monitored over time. To verify the specificity of QST-GAL, an inhibition experiment was conducted. Cells were pre-incubated with 5 mM D-galactose for 30 min and then incubated with 10 μM QST-GAL. Fluorescence signals were observed using a laser scanning confocal microscope ($\lambda_{ex} = 500$ nm, $\lambda_{em} = 700$ nm).

Detection of palbociclib-induced cellular senescence. To simulate the senescence process induced by palbociclib, 4T1 cells were treated with 5 μM palbociclib for 7 days. The morphology of the cells was continuously monitored until they exhibited the typical characteristics of cellular senescence. The treated cells were then subjected to time-lapse imaging using 10 μM QST-GAL as a probe.

Immunofluorescence detection of senescence-associated markers. To further confirm senescence induced by palbociclib, the expression of senescence-associated markers p16 and Lamin B1 was assessed using immunofluorescence staining [33–35]. Both control and palbociclib-treated cells were fixed with 2 % paraformaldehyde (PFA) for 15 min and then thoroughly washed with PBS. Cells were then blocked with a blocking buffer (10 % serum and 0.2 % Triton) for 1 h at room temperature to prevent non-specific binding. The cells were then incubated with primary antibodies against p16 and Lamin B1 overnight at 4℃. After washing, the cells were further incubated with fluorescently labeled secondary antibodies at room temperature for 1 h. Images were captured using a confocal microscope.

Co-localization analysis of QST-GAL with markers. To examine the co-localization of QST-GAL with p16 and Lamin B1, 10 μM QST-GAL was incubated with immuno-stained cells for 30 min at 37℃. After thoroughly washing, the cells were imaged immediately using a laser scanning confocal microscope.

Lysosomal co-localization experiments. To further validate the subcellular localization of QST-GAL, we conducted additional lysosomal co-localization experiments. 10 μM QST-GAL and the commercial lysosomal tracker Lyso-Tracker was incubated with cells for 30 min at 37℃. After thoroughly washing, the cells were imaged immediately using a laser scanning confocal microscope.

2.4. Establishment of mouse models

All animal experiments were conducted in accordance with the ethical guidelines set by the Institutional Animal Care and Use Committee (IACUC) of Jilin University under the animal experimental ethical inspection permit number SY202409006. A series of disease models were established using BALB/c-nu mice as follows:

Ectopic tumor mouse model. 4T1 cells were used to establish a breast cancer model in BALB/c-nu mice. Specifically, 100 μL of cell suspension (containing 0.5×10^6 cells) was subcutaneously injected into the dorsal region of female BALB/c-nu mice [36]. The mouse model was successfully established after 7 days. Before imaging, mice were anesthetized by inhaling 2 % isoflurane and *in situ* injected with QST-GAL. Imaging was conducted using a small animal imaging system ($\lambda_{ex} = 535$ nm; $\lambda_{em} = 680$ nm). After imaging, the mice were euthanized, and their tumors and major organs (lung, liver, kidney, spleen, and heart) were collected for another imaging using an imaging system.

Orthotopic tumor mouse model. 4T1 cells were also used to generate the orthotopic tumor mouse model [30]. A 100 μL cell suspension (containing 0.5×10^6 cells) was subcutaneously injected into the left mammary fat pad of female BALB/c-nu mice. To simulate cancer chemotherapy, the mice were administered with a single oral dose of palbociclib at various concentrations (0, 10, 50, 100, and 150 mg/kg) [36]. Tumor volume was monitored over 7 days. After 7 days, the mice were subjected to imaging. Mice were anesthetized with 2 % isoflurane and then intraperitoneally (i.p.) injected with QST-GAL. Images were taken every 2 min for 30 min using a small animal imaging system ($\lambda_{ex} = 535$ nm; $\lambda_{em} = 680$ nm). Following imaging, the mice were euthanized, and their tumors and major organs (lung, liver, kidney, spleen, and heart) were collected for another round of imaging using an imaging system.

3. Results and discussion

3.1. Analytical performance of QST-GAL

A β-gal-specific fluorescence probe was synthesized using QST-OH as the fluorophore and D-galactose as the recognition group. To validate the feasibility of the probe and to evaluate its ability to selectively detect β-gal activity, *in vitro* experiments were first conducted.

Firstly, the spectral properties of QST-OH and its precursor QST-GAL were investigated (Figure S13A). QST-GAL showed no significant absorption in the visible range, whereas QST-OH displayed a distinct absorption peak centered at 460 nm with a molar extinction coefficient ($\varepsilon_{460} = 9.12\ \text{mM}^{-1}\cdot\text{cm}^{-1}$), indicating effective π–π^* transition. As shown in Figure S13B, QST-OH exhibited a strong fluorescence emission at 710 nm with an absolute quantum yield of 0.10, while QST-GAL remained nearly non-fluorescent ($\Phi < 0.01$), demonstrating the excellent fluorogenic response upon enzymatic activation.

To optimize experimental conditions, we evaluated several key parameters, including pH and temperature. Detailed discussions are provided in the Supplementary Material. The optimal conditions were determined to be pH 7.4, and a temperature of 37℃ (Figure S14).

And then the reaction time was optimized under this condition by dissolving 10 U/mL β-gal and 10 μM QST-GAL in PBS buffer solution (10 mM, pH 7.4) and incubating at 37℃ for different reaction times (0.3, 0.6, 0.9, 1.2, 1.5, 2.5, 3, 4, 5 and 10 min). The optimal reaction time was determined based on the change in fluorescence signal. As shown in Fig. 2A, in the presence of β-gal (10 U/mL), the fluorescence intensity ($\lambda_{em} = 710$ nm) of the probe solution gradually increased with the reaction time and reached the maximum value at 3 min, and then the fluorescence intensity reached equilibrium. In order to fully ensure the complete reaction of the enzymatic reaction, 5 min was chosen as the optimal reaction time in this paper. In addition, as shown in Figure S15, the fluorescence signals of both the fluorophore QST-OH and the probe QST-GAL remained stable over a period of 120 min, confirming their good chemical and photostability under physiological conditions.

13–30: Cations (Ag^+, Al^{3+}, Ba^{2+}, Ca^{2+}, Cd^{2+}, Co^{2+}, Cu^{2+}, Fe^{2+}, Fe^{3+}, Hg^{2+}, K^+, Li^+, Mg^{2+}, Mn^{2+}, Na^+, Ni^{2+}, Pb^{2+}, Zn^{2+}); 31–48: Amino acids and thiol-containing biomolecules (Asp, Cys, GSH, Hcy, His, Ser, Tyr, Val, Phe, Ala, Met, Gly, Glu, Arg, Lys, Leu, NAC, Thr); 49–55: Enzymes (Butyrylcholinesterase (BChE, 12 U/mL), Carboxylesterase 2 (CES2, 1 μg/mL), γ-Glutamyltransferase (GGT, 20 U/L), Dipeptidyl Peptidase-4 (DPP4, 50 μg/mL), N-Acetyl-β-D-glucosaminidase (NAG, 10 U/mL), β-Glucuronidase (GLU, 10 U/mL), and β-galactosidase (β-gal, 10 U/mL)).

Under these conditions, the linear relationship between fluorescence intensity ($\lambda_{ex} = 585$ nm, $\lambda_{em} = 710$ nm) and β-gal concentration was investigated. As shown in Fig. 2B, the fluorescence intensity increased with rising β-gal concentrations. Notably, a strong linear correlation ($R^2 = 0.998$) was observed at the β-gal concentration range of 2–28 U/mL, demonstrating the probe's high sensitivity. We also assessed the limit of detection (LOD) of QST-GAL and found it to be exceptionally low at

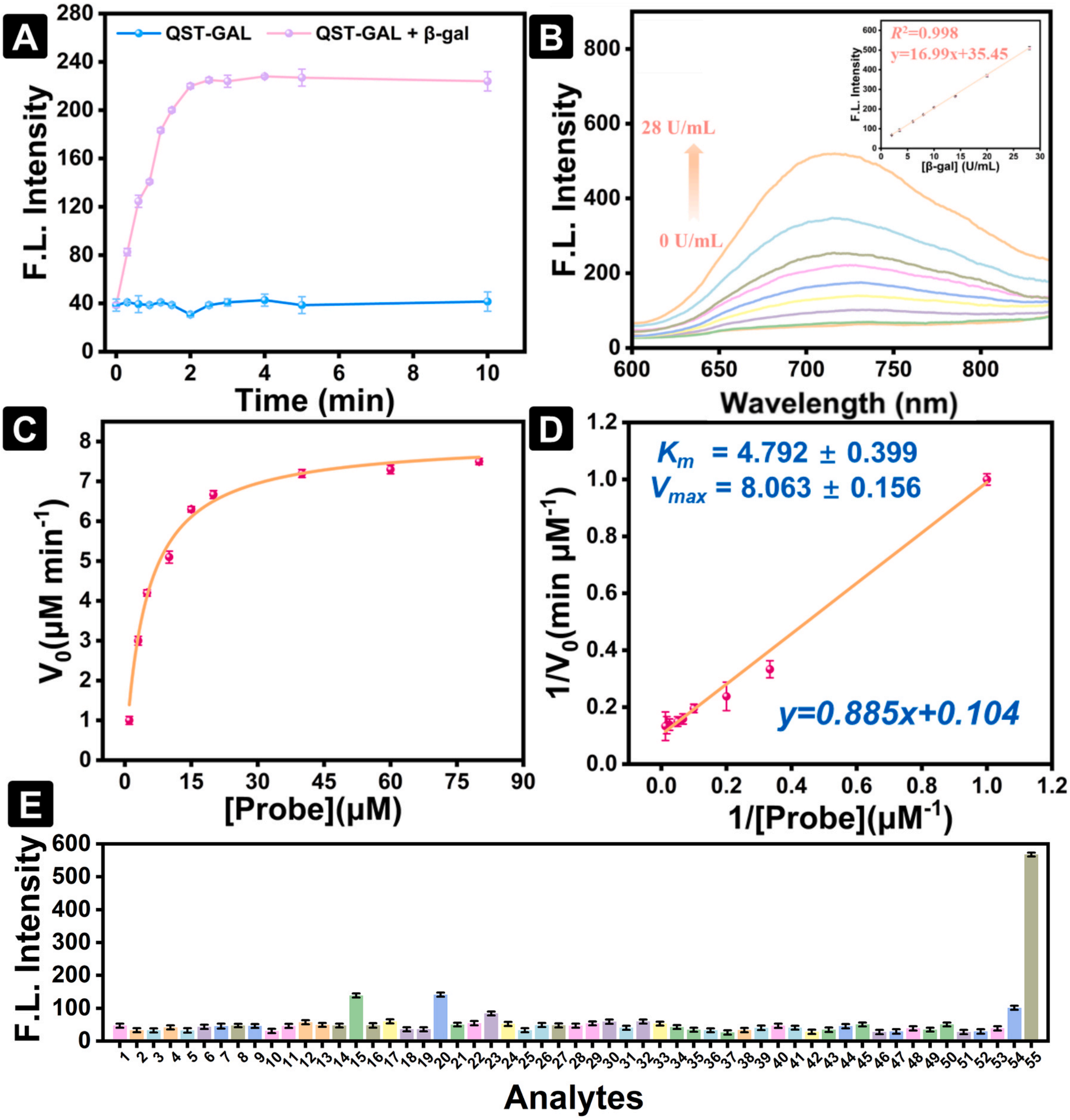

Fig. 2. (A) Time-dependent fluorescence intensity of QST-GAL (10 μM, $\lambda_{ex} = 585$ nm, $\lambda_{em} = 710$ nm) in the presence or absence of β-gal (10 U/mL). (B) Fluorescence spectra of QST-GAL (10 μM) upon incubation with increasing concentrations of β-gal (0–28 U/mL), monitored at $\lambda_{em} = 710$ nm. (C) Michaelis–Menten plot for the enzymatic reaction between β-GAL (10 U/mL) and QST-GAL at varying substrate concentrations (1, 3, 5, 10, 15, 20, 40, 60, and 80 μM). (D) Lineweaver–Burk plot derived from the same kinetic data. (E) Fluorescence response of QST-GAL (10 μM) to various potential interfering species (1 mM unless otherwise specified). Compounds tested: 1–12: Anions (Br^-, $ONOO^-$, Cl^-, ClO^{4-}, CN^-, F^-, $H_2PO_4^-$, HPO_4^{2-}, HSO_4^-, I^-, SCN^-, SO_3^{2-});.

0.377 U/mL. The methodology for LOD calculation is detailed in the Supplementary Material.

Subsequently, the enzyme kinetics between QST-GAL and β-gal were investigated using Michaelis-Menten and Lineweaver-Burk (Fig. 2C and D). The maximum reaction velocity (V_{max}) was determined to be 8.063 μM min^{-1}, the Michaelis constant (K_m) was 4.792 μM and the enzyme catalytic constant (K_{cat}) is 0.806 min^{-1} . These kinetic parameters reflected the high affinity and efficient catalytic effect between QST-GAL and β-gal. To evaluate the selectivity to β-gal, we tested QST-GAL in the presence of various potential interferents, including amino acids,

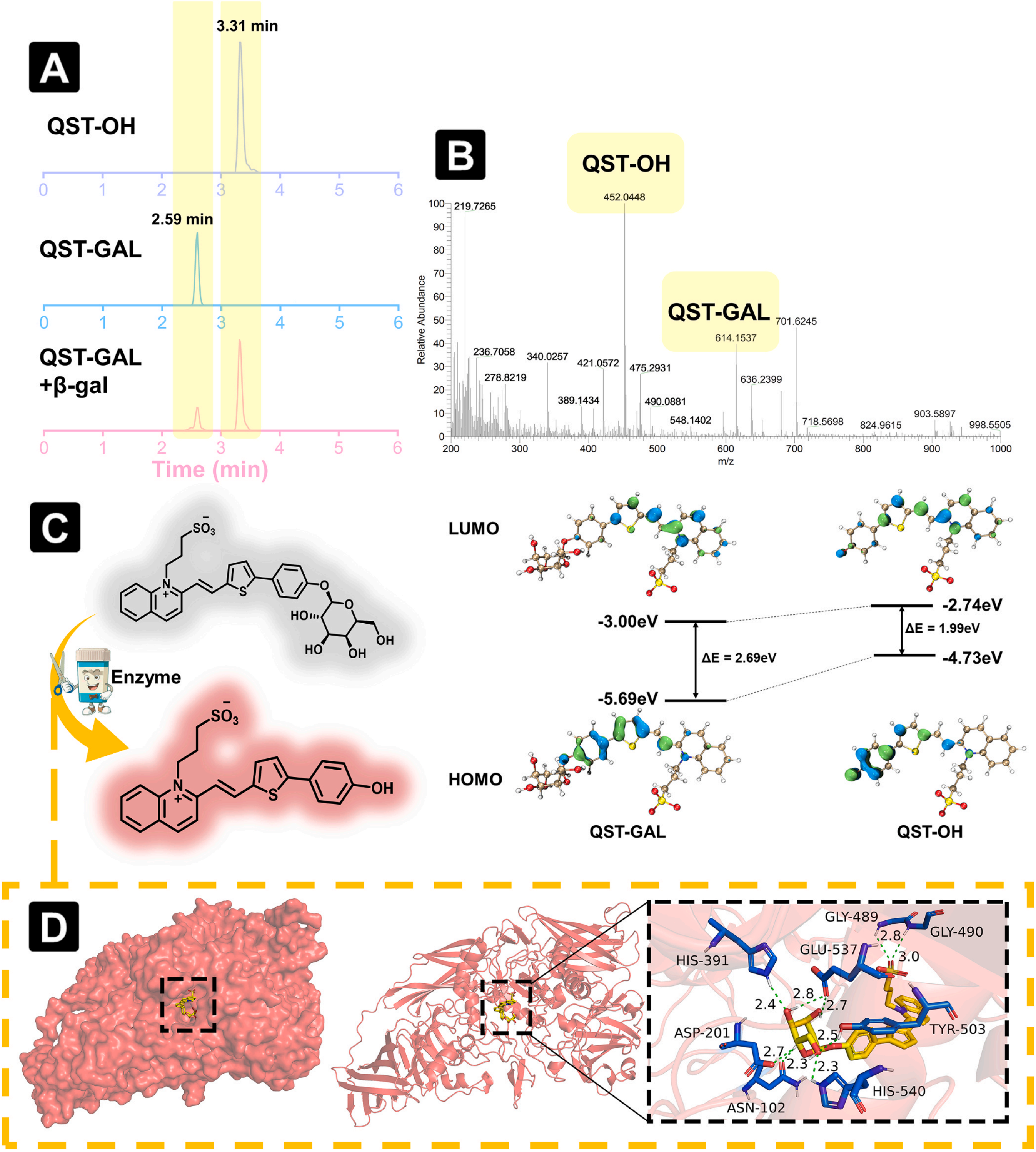

Fig. 3. (A) HPLC-MS analysis of the reaction mixture, showing retention times of QST-OH (RT = 3.31 min) and QST-GAL (RT = 2.59 min). (B) Mass spectrometric analysis of the reaction mixture, with observed m/z values for QST-OH (452.0448) and QST-GAL (614.1537). (C) Schematic representation of enzymatic hydrolysis (left), and the calculated HOMO–LUMO energy gaps of QST-OH (ΔE = 1.99 eV) and QST-GAL (ΔE = 2.69 eV) (right). (D) Molecular docking simulation of QST-GAL binding to β-gal, with the right panel highlighting seven key hydrogen bonds involving residues ASN102, ASP201, HIS391, GLY489, GLY490, TYR503, GLU537, and HIS540.

metal ions, anions, and thiols (Fig. 2E). The probe showed high selectivity for β-gal. These results demonstrate the high sensitivity of QST-GAL to β-gal, reinforcing its potential for sensitive and specific β-gal detection. In addition, a systematic comparison was made between the performance of this probe and that of previous probes. As shown in the Table S1, while ensuring that basic in vitro testing requirements are met, this probe demonstrates faster response speed and shorter response time, fully highlighting its performance advantages over previous probes.

3.2. *Spectral properties and reaction mechanism*

According to the above results have been found that, QST-GAL did not exhibit a noticeable fluorescence signal initially. However, upon the addition of β-gal, the fluorescence intensity gradually increased, with the emission peak shift resembling that of QST-OH (Fig. 2B). Based on this observation, we hypothesize that, under the catalysis of β-gal, QST-GAL undergoes hydrolysis, leading to the release of the hydroxyl group in the D-π-A structure, which acts as a strong electron donor. This reaction enhances the intramolecular charge transfer (ICT) effect, which significantly increases the fluorescence intensity. Specifically, the hydrolysis reaction facilitates the release of the phenolic hydroxyl group from QST-GAL, thereby enhancing the ICT effect and leading to a substantial increase in the fluorescence intensity at 710 nm.

To further validate these findings, we performed a high-performance liquid chromatography-mass spectrometry (HPLC-MS) analysis of the reaction. Initially, without β-gal, mass spectrometry revealed only the signal of QST-GAL. After the addition of β-gal, the signals of both QST-OH and QST-GAL appeared, but the QST-OH signal was more prominent (Fig. 3A). To further confirm this result, we conducted additional analysis by liquid chromatography-mass spectrometry. The retention times for QST-OH and QST-GAL were found to be 3.31 min and 2.59 min, respectively (Fig. 3B). Two distinct chromatographic peaks corresponding to QST-OH and QST-GAL were also observed at these retention times. Taken together, the HPLC-MS analysis further confirmed the enzyme-mediated reaction mechanism.

Subsequently, these results were further validated by theoretical calculations. We initially performed calculations on both QST-OH and QST-GAL. The HOMO-LUMO energy gap of QST-GAL was 2.69 eV, whereas that of QST-OH was 1.99 eV. The larger HOMO-LUMO energy gap in QST-GAL can cause a marked reduction in internal electron transfer efficiency, in turn diminishing the ICT effect, resulting in weak fluorescence emission. In contrast, upon being hydrolyzed by β-gal, the recognition group in QST-GAL is cleaved and replaced by a hydroxyl group (Fig. 3C). Hydroxyl groups are known to have strong electron-donating properties and thus can enhance the electron density of the molecule. This substitution leads to a more efficient internal electron transfer because the electron-donating hydroxyl group facilitates smoother electron movement across the molecule. As a result, the ICT effect is restored, in turn allowing fluorescence signals to be significantly enhanced.

Furthermore, molecular docking simulations were performed using Autodock. As shown in Fig. 3D, the docking simulation indicates that ASN102, ASP201, HIS391, GLY489, GLY490, TYR503, GLU537 and HIS540 residues in QST-GAL form nine hydrogen bonds with β-gal. The calculated binding energy was −8.6 kcal/mol, which is demonstrative of a strong binding affinity between QST-GAL and β-gal and an effective interaction between the probe and the target enzyme. These results collectively confirm that the QST-GAL probe can efficiently bind to β-gal and subsequently undergo hydrolysis to generate QST-OH that leads to fluorescence recovery.

3.3. *Fluorescence imaging of drug-induced cellular senescence*

The cell viability of QST-GAL and QST-OH were evaluated using the CCK-8 assay. The results indicated that the cell survival rate exceeded 85 % (Figure S16A and Figure S17A), suggesting that QST-GAL and QST-OH have low cytotoxicity. Hemolysis tests further confirmed that QST-GAL and QST-OH exhibited a low hemolysis rate, demonstrating its high biocompatibility (Figure S16B and Figure S17B).

In the validation of the capability of QST-GAL in monitoring cellular senescence, we first assessed its performance and specificity in imaging endogenous β-gal. In the experiments, we imaged breast cancer cells using the QST-GAL probe. The results showed that the fluorescence signal in the cells increased over time, indicating that the probe effectively labels breast cancer cells (Fig. 4A, Figure S18A). To confirm that the fluorescence signal originated from β-gal activity, we introduced the D-galactose (a β-gal inhibitor) into the experiment. The results revealed that, compared to the control group, the fluorescence intensity in the inhibitor-treated group significantly decreased, verifying the high specificity of the QST-GAL probe for endogenous β-gal (Figure S18B).

A cellular senescence model was established by treating breast cancer cells with palbociclib, a chemotherapeutic drug known to induce cell cycle arrest and trigger cellular senescence. Treated cells exhibited typical senescence-associated morphological changes such as increased cell size, a flattened shape, and nuclear structural alterations. X-GAL staining is a classical method to validate the establishment of senescent cell models. As shown in Figure S19E, cells were stained using X-GAL and a blue signal was observed in senescent cells but not in normal cells, confirming the success of the model construction. To further validate the subcellular localization of QST-GAL, we conducted additional lysosomal co-localization experiments. Specifically, both the cell lines used in this study and the drug-induced senescent cell model were co-stained with the commercial lysosomal tracker Lyso-Tracker. As shown in Figure S19, QST-GAL exhibited a high degree of overlap with Lyso-Tracker in both cell types, with Pearson correlation coefficients of 0.843 and 0.787, respectively. These results indicate that QST-GAL possesses good lysosomal targeting capability.

To further validate the reliability of our findings, we correlated the probe detection results with well-established cellular senescence markers at the single-cell level. Immunostaining was employed to assess the changes in the expression of senescence markers, p16 and Lamin B1. Since β-gal activity remains intact after fixation, both palbociclib-treated and untreated breast cancer cells were fixed with paraformaldehyde before immunostaining. The QST-GAL probe was then co-applied, and its fluorescence signals were recorded after 30 min. The results showed a significant increase in red fluorescence from QST-GAL in senescent cells, accompanied by a marked decrease in Lamin B1 expression and a notable increase in p16 expression (Fig. 4B). Moreover, the fluorescence intensity of QST-GAL was positively correlated with p16 expression levels. These findings collectively confirm that the QST-GAL probe is a reliable indicator of senescence-associated β-gal activity and can effectively assess cellular senescence status.

3.4. *Fluorescence imaging in mice models of breast cancer and senescence*

To evaluate the *in vivo* imaging potential of the QST-GAL probe, a breast cancer ectopic tumor model was established. After the tumor was established in the dorsal region of mice, the QST-GAL probe was directly injected into the tumor site, with the same dosage administered to the corresponding location in the control group. As shown in Fig. 5A, a significant fluorescence signal was observed at the tumor site. With this fluorescence-guided imaging, the tumor was surgically excised, and the complete removal of all highly fluorescent regions was ensured. To further characterize the presence of normal tissues within the excised samples, histological analysis was performed using hematoxylin and eosin (HE) staining. As illustrated in Figure S20A, the excised tissue consisted mainly of tumor cells, with only a minimal presence of normal tissue at the periphery. In conclusion, the QST-GAL probe successfully *in situ* imaged breast cancer in mice and for facilitating precise surgical resection. It shows promise as a tool for clinical tumor surgery assistance.

Next, we implanted 4T1 cells into the left mammary fat pad of young

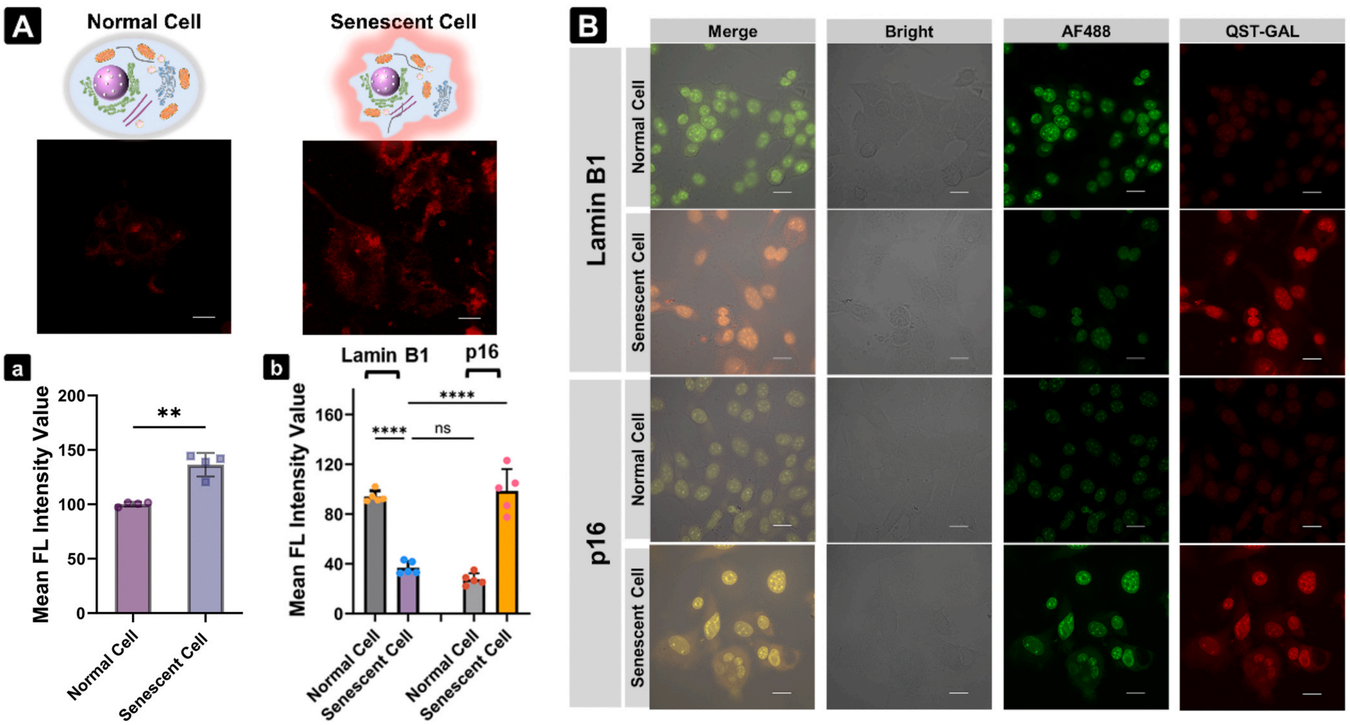

Fig. 4. (A) Schematic diagram of the cell testing process. Fluorescence imaging graphs of normal breast cancer cells (a) and drug-induced senescent breast cancer cells (b), and the corresponding bar graph for quantitative analysis (c). (d) Quantitative bar graph of immunofluorescence data. (B) Immunofluorescence data graph (Lamin B1 and p16 were selected as two aging biomarkers, and AF488 was a fluorescent label dye for secondary antibodies). (*$P \leq 0.05$; ** $P \leq 0.01$; *** $P \leq 0.001$; **** $P \leq 0.0001$, data analyses were performed on independent samples with equal variances; data are means ± SD; n = 5). Scale bar = 20 μm.

female BALB/c-nu mice to establish an orthotopic breast cancer model. Palbociclib was then orally administered at doses of 0, 10, 50, 100, and 150 mg/kg for 7 days. Tumor volume significantly decreased with increasing drug concentration, which was observed visually. Fluorescence imaging was performed using the QST-GAL probe which was administered via intraperitoneal injection. Fluorescence intensity was observed to increase significantly with increasing drug concentration, indicating a positive correlation between drug concentration and senescence-induced fluorescence signals. This fluorescence signal reflects the cellular senescence induced by the drug, with the probe selectively detecting senescent cells. As shown in Fig. 5B, higher palbociclib concentrations led to tumor volume reduction and intensified fluorescence signals (Figure S21), demonstrating a positive correlation between QST-GAL and palbociclib treatment. These findings highlight the QST-GAL probe as a valuable tool for assessing the therapeutic efficacy of palbociclib in breast cancer treatment. Following euthanasia, major organs and tumor tissues were collected for fluorescence imaging. As shown in Figure S20B, significant fluorescence signals were detected in the liver and intestines, as well as in the bladder and kidneys, further confirming the altered hydrophilicity of the probe.

Furthermore, HE staining was performed on tumor tissues. As shown in the Figure S20, in the tumor cells that did not receive drug treatment, the nuclei were deeply stained and the nucleoplasmic ratios were obviously enlarged, showing typical tumor cell characteristics. When the drug concentration was 10 mg/kg, a small number of cells began to show senescence-related morphological features, but the overall effect was mild. When the concentration was increased to 50 mg/kg, the number of senescent cells increased significantly and the cell morphology gradually changed. When the concentration was further increased to 100 mg/kg, the senescence characteristics of the cells were obvious, and some cells began to show apoptosis characteristics. When the drug concentration reached 150 mg/kg, the cell morphology was obviously collapsed and crumpled, the chromatin was highly concentrated, and a large number of cells entered the apoptotic state. Overall, as the concentration of the drug increased, the tumor cells gradually went from proliferation inhibition, senescence aggravation to apoptosis, indicating that the drug can significantly inhibit the growth of tumor cells and induce cellular senescence and apoptosis at high concentrations. In summary, the QST-GAL probe demonstrates a strong positive correlation with palbociclib and serves as an effective tool not only for breast cancer imaging but also for evaluating the therapeutic efficacy of palbociclib in breast cancer treatment.

4. Conclusion

In conclusion, we designed and synthesized QST-GAL, an enzyme-responsive fluorescence probe for the sensitive detection of β-gal. The probe had excellent imaging capabilities in complex physiological environments. By introducing a sulfonic acid group to enhance its hydrophilicity, we improved the probe's sensitivity and successfully enabled the "off-on" ICT effect, resulting in low-background fluorescence. *In vitro* and cellular assays confirmed that QST-GAL effectively imaged breast cancer cells and monitored drug-induced cellular senescence. In *in vivo* experiments, the probe successfully facilitated tumor imaging in a breast cancer mouse model and indirectly assessed the chemotherapy efficacy. These findings highlight the potential of QST-GAL as a powerful tool for imaging and early diagnosis of breast cancer. With its excellent cellular senescence imaging capacity, QST-GAL can be used to effectively monitor the therapeutic effects of palbociclib in breast cancer chemotherapy.

CRediT authorship contribution statement

Jingkang Li: Writing – original draft, Validation, Investigation, Data curation, Conceptualization. **Lanyun Zhang:** Investigation. **Wanqi Li:** Investigation. **Chen Zhao:** Investigation, Data curation. **Mo Ma:** Investigation, Data curation. **Daqian Song:** Supervision, Resources, Project administration, Funding acquisition. **Pinyi Ma:** Writing – review &

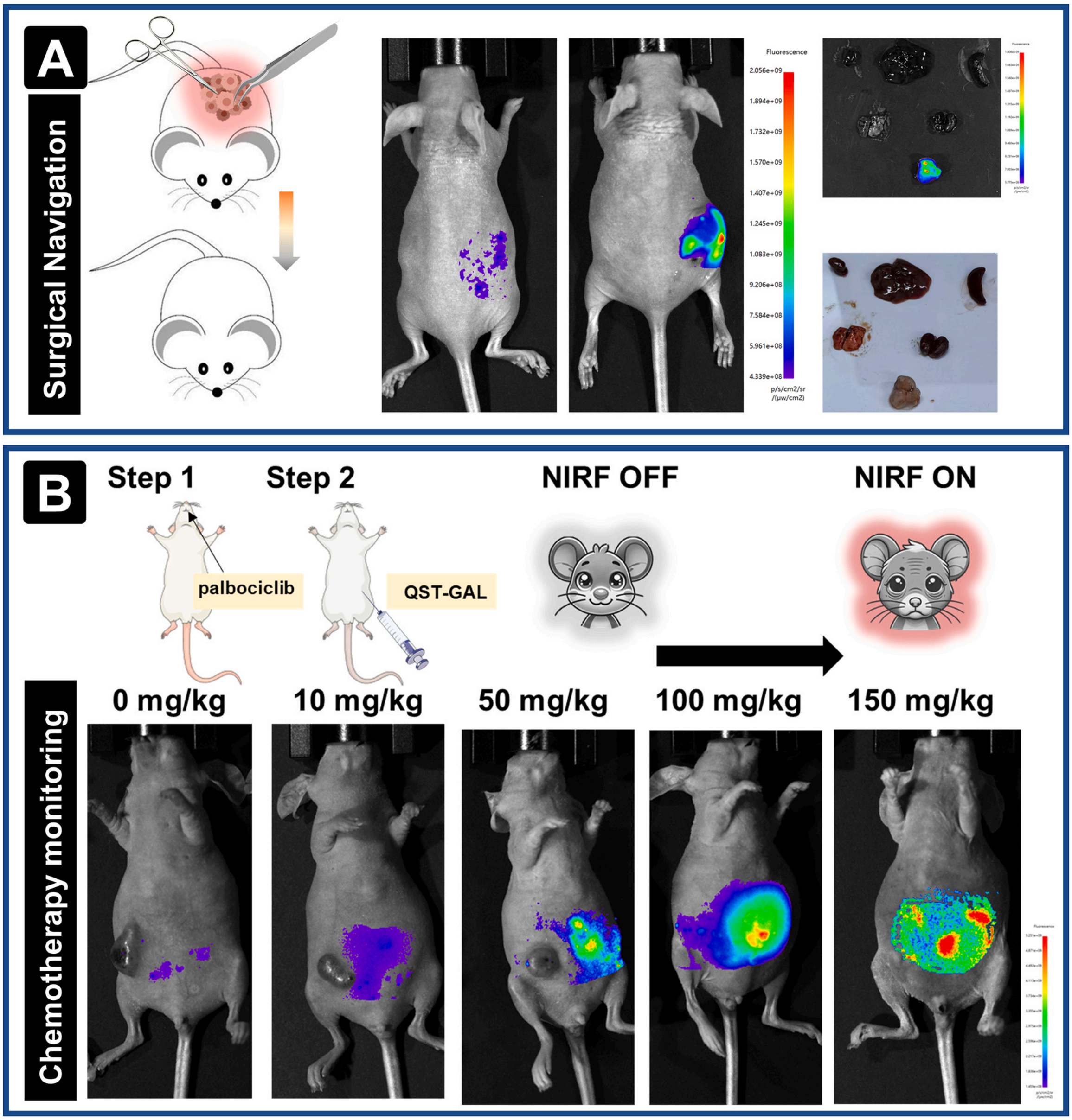

Fig. 5. (A) Fluorescence-guided tumor resection and corresponding anatomical illustrations. (a) Fluorescence image of the control group (QST-GAL was injected *in situ* at the same anatomical site on the right side without tumor). (b) Fluorescence image of tumor-bearing mice following *in situ* injection of QST-GAL at the tumor site. (c) Fluorescence images of major organs excised from tumor-bearing mice. (d) Bright-field photograph of the corresponding major organs. (I: Heart, II: Liver, III: Spleen, IV: Lung, V: Kidney, VI: Tumor). (B) Fluorescence images of an *in situ* breast cancer mouse model after 7 days of treatment with palbociclib at doses of 0, 10, 50, 100, and 150 mg/kg. The upper part of the figure presents a schematic illustration: Step 1 simulates the aging process induced by oral administration of palbociclib in breast cancer-bearing mice; Step 2 depicts the fluorescence imaging procedure following intraperitoneal injection of the probe.

editing, Project administration, Data curation. **Qiong Wu:** Writing – review & editing, Resources, Project administration, Investigation.

Declaration of Competing Interest

The authors declare that they have no known competing financial interests or personal relationships that could have appeared to influence the work reported in this paper.

Acknowledgements

This work was supported by the National Natural Science Foundation of China (22004046 and 22074052), the Science and Technology Developing Foundation of Jilin Province of China (20240404044ZP), and the Jilin Province Health Science and Technology Capability Improvement Plan Project (2022LC121).

Appendix A. Supporting information

Supplementary data associated with this article can be found in the online version at doi:10.1016/j.snb.2025.138418.

Data availability

Data will be made available on request.

References

[1] J.L. Caswell-Jin, L.P. Sun, D. Munoz, Y. Lu, Y.S. Li, H. Huang, et al., Analysis of breast cancer mortality in the US-1975 to 2019, JamaJ. Am. Med. Assoc. 331 (2024) 233–241.

[2] K.P. Trayes, S.E.H. Cokenakes, Breast cancer treatment, Am. Fam. Physician 104 (2021) 171–178.

[3] S. Loibl, P. Poortmans, M. Morrow, C. Denkert, G. Curigliano, Breast cancer, Lancet 397 (2021) 1750–1769.

[4] N. Harbeck, F. Penault-Llorca, J. Cortes, M. Gnant, N. Houssami, P. Poortmans, et al., Breast cancer, Nat. Rev. Dis. Prim. 5 (2019) 66.

[5] E.I. Obeagu, G.U. Obeagu, Breast cancer: a review of risk factors and diagnosis, Medicine 103 (2024) e36905.

[6] A.G. Waks, E.P. Winer, Breast cancer treatment a review, JamaJ. Am. Med. Assoc. 321 (2019) 288–300.

[7] V. Giannakeas, D.W. Lim, S.A. Narod, Bilateral mastectomy and breast cancer mortality, Jama Oncol. 10 (2024) 1228–1236.

[8] T. Saleh, S. Bloukh, M. Hasan, S.Al Shboul, Therapy-induced senescence as a component of tumor biology: evidence from clinical cancer, Biochim. Et. Biophys. ActaRev. Cancer 1878 (2023) 188994.

[9] U. Harjes, Tumour biomarkers: a mark is a marker, Nat. Rev. Cancer 17 (2017) 708.

[10] L.Y. Jiang, X.Y. Lin, F.H. Chen, X.Y. Qin, Y.X. Yan, L.J. Ren, et al., Current research status of tumor cell biomarker detection, Microsyst. Nanoeng. 9 (2023) 123.

[11] Y.M. Shan, L.N. Zhang, S.X. Wu, X.L. Li, H. Zhang, F.F. Xiang, et al., Revelation of fl-galactosidase variation in senile sperms and organs via a silicon xanthene near-infrared probe, Sens Actuators B Chem. 397 (2023) 134663.

[12] Y.S. Cai, H.H. Zhou, Y.H. Zhu, Q. Sun, Y. Ji, A.Q. Xue, et al., Elimination of senescent cells by β-galactosidase-targeted prodrug attenuates inflammation and restores physical function in aged mice, Cell Res. 30 (2020) 574–589.

[13] Y. Gao, Y.L. Hu, Q.M. Liu, X.K. Li, X.M. Li, C.Y. Kim, et al., Two-dimensional design strategy to construct smart fluorescent probes for the precise tracking of senescence, Angew. Chem. Int Ed. 60 (2021) 10756–10765.

[14] K.Z. Gu, Y.S. Xu, H. Li, Z.Q. Guo, S.J. Zhu, S.Q. Zhu, et al., Real-time tracking and in vivo visualization of β-galactosidase activity in colorectal tumor with a ratiometric near-infrared fluorescent probe, J. Am. Chem. Soc. 138 (2016) 5334–5340.

[15] C.H. Wu, J. van Riggelen, A. Yetil, A.C. Fan, P. Bachireddy, D.W. Felsher, Cellular senescence is an important mechanism of tumor regression upon c-Myc inactivation, Proc. Natl. Acad. Sci. 104 (2007) 13028–13033.

[16] Z.N. Dong, Y.H. Luo, Z.C. Yuan, Y. Tian, T.Q. Jin, F. Xu, Cellular senescence and SASP in tumor progression and therapeutic opportunities, Mol. Cancer 23 (2024) 181.

[17] D.V. Faget, Q.H. Ren, S.A. Stewart, Unmasking senescence: context-dependent effects of SASP in cancer, Nat. Rev. Cancer 19 (2019) 439–453.

[18] C.A. Schmitt, UnSASPing senescence: unmasking tumor suppression, Cancer Cell 34 (2018) 6–8.

[19] L.L. Xu, H.Y. Chu, D.J. Gao, Q. Wu, Y. Sun, Z.X. Wang, et al., Chemosensor with ultra-high fluorescence enhancement for assisting in diagnosis and resection of ovarian cancer, Anal. Chem. 95 (2023) 2949–2957.

[20] X.Z. Luo, E.Z. Hu, F. Deng, C.L. Zhang, Y.Z. Xian, A dual-enzyme activated fluorescent probe for precise identification of tumor senescence, Chem. Sci. (2025) 6507–6514.

[21] H.F. Wang, Y.L. Zhuang, S.Y. Fu, Y.X. Shen, H.J. Qian, X.Q. Yan, et al., Modular and fast assembly of self-immobilizing fluorogenic probes for β-galactosidase detection, Anal. Chem. 96 (2024) 18939–18945.

[22] K.C. Zhao, H.L. Tan, C. Fang, Z.L. Zhou, C.Y. Wu, X.H. Zhu, et al., An activatable fluorescence probe for rapid detection and in situ imaging of β-galactosidase activity in cabbage roots under heavy metal stress, Food Chem. 452 (2024) 139557.

[23] J.K. Li, M. Ma, Z.M. Zhang, L.L. Xu, B. Yang, Q.P. Diao, et al., A novel carboxylesterase 2-targeted fluorescent probe with cholic acid as a recognition group for early diagnosis of drug- and environment-related liver diseases, J. Hazard Mater. 480 (2024) 135966.

[24] S.Q. Zhang, M. Ma, J.K. Li, J.X. Li, L.L. Xu, D.J. Gao, et al., A pyroglutamate aminopeptidase 1 responsive fluorescence imaging probe for real-time rapid differentiation between thyroiditis and thyroid cancer, Anal. Chem. 96 (2024) 5897–5905.

[25] Z.W. Zheng, X. Dai, X.Y. Li, C. Du, PCL-based and hirudin-containing composite nanofibers for prolonged anticoagulation effect, Chem. Res. Chin. Univ. 39 (2023) 1023–1030.

[26] S.S. Zhang, M. Zhang, Y. Guo, Highly sensitive ethanol gas sensor based on Ag nanoparticles decorated In2O3, Chem. Res. Chin. Univ. 40 (2024) 1033–1040.

[27] R.L. Liu, H.Y. Chen, S.L. Zhang, B. Zhao, L. Zhou, F. Zhang, et al., Engineered water-soluble photosensitive fluorescent probes of β-galactosidase with fast response based on triarylboron compound derivatives for ovarian cancer cell imaging, Sens Actuators B Chem. 372 (2022) 132660.

[28] C.M. Liu, Y. Mei, H.F. Yang, Q. Zhang, K. Zheng, P. Zhang, et al., Ratiometric fluorescent probe for real-time detection of β-galactosidase activity in lysosomes and its application in drug-induced senescence imaging, Anal. Chem. 96 (2024) 3223–3232.

[29] M.Y. Yu, Z.Q. Meng, S.J. Yi, J.J. Chen, W.P. Xu, B.K. Ruan, et al., A β-galactosidase-activated fluorogenic reporter for the detection of gastric cancer in vivo and in urine, Anal. Chem. 96 (2024) 6390–6397.

[30] Q. Wu, Q.H. Zhou, W. Li, T.B. Ren, X.B. Zhang, L. Yuan, Evolving an ultra-sensitive near-infrared β-galactosidase fluorescent probe for breast cancer imaging and surgical resection navigation, ACS Sens. 7 (2022) 3829–3837.

[31] J.L. Li, L.L. Wang, X.Y. Luo, Y.H. Xia, Y.Q. Xie, Y.L. Liu, et al., Dual-parameter recognition-directed design of the activatable fluorescence probe for precise imaging of cellular senescence, Anal. Chem. 95 (2023) 3996–4004.

[32] X.P. Fan, J. Huang, T.B. Ren, L. Yuan, X.B. Zhang, De novo design of activatable photoacoustic/fluorescent probes for imaging acute lung injury in vivo, Anal. Chem. 95 (2023) 1566–1573.

[33] X. Zhang, V.M. Pearsall, C.M. Carver, E.J. Atkinson, B.D.S. Clarkson, E.M. Grund, et al., Rejuvenation of the aged brain immune cell landscape in mice through p16-positive senescent cell clearance, Nat. Commun. 13 (2022) 5671.

[34] L.P. Deng, R.T. Ren, Z.P. Liu, M.S. Song, J.Y. Li, Z.M. Wu, et al., Stabilizing heterochromatin by DGCR8 alleviates senescence and osteoarthritis, Nat. Commun. 10 (2019) 3329.

[35] A.M. Garrido, A. Kaistha, A.K. Uryga, S. Oc, K. Foote, A. Shah, et al., Efficacy and limitations of senolysis in atherosclerosis, Cardiovasc. Res. 118 (2022) 1713–1727.

[36] S. Rojas-Vázquez, B. Lozano-Torres, A. García-Fernández, I. Galiana, A. Perez-Villalba, P. Martí-Rodrigo, et al., A renal clearable fluorogenic probe for in vivo β-galactosidase activity detection during aging and senolysis, Nat. Commun. 15 (2024) 775.

Jingkang Li is currently a PhD student in College of Chemistry, Jilin University. His interest is spectral analysis.

Chen Zhao is currently a PhD student in College of Chemistry, Jilin University. Her interest is spectral analysis.

Mo Ma is currently a PhD student in School of Pharmacy, Jilin University. His interest is spectral analysis.

Lanyun Zhang is currently a master degree student in College of Chemistry, Jilin University. Her interest is spectral analysis.

Wanqi Li is currently a master degree student in College of Chemistry, Jilin University. Her interest is spectral analysis.

Pinyi Ma received his doctor's degree from College of Chemistry, Jilin University in 2017 and he is an associate professor in that school. His research area is spectral analysis.

Qiong Wu received her doctor's degree from College of Chemistry, Jilin University in 2018 and she is an associate professor in The Third Bethune Hospital of Jilin University. Her research area is spectral analysis and biosensor.

Daqian Song received his doctor's degree from College of Chemistry, Jilin University in 2003 and he is a professor in that school. His research areas are spectral and chromatography analysis.